



# Carbon dioxide adsorption and interaction with formation fluids of Jordanian unconventional reservoirs

H. Samara<sup>1</sup> · T. V. Ostrowski<sup>2</sup> · F. Ayad Abdulkareem<sup>3</sup> · E. Padmanabhan<sup>3,4</sup> · P. Jaeger<sup>1</sup>

Received: 2 August 2021 / Accepted: 13 October 2021 / Published online: 29 October 2021  
© The Author(s) 2021

## Abstract

Shales are mostly unexploited energy resources. However, the extraction and production of their hydrocarbons require innovative methods. Applications involving carbon dioxide in shales could combine its potential use in oil recovery with its storage in view of its impact on global climate. The success of these approaches highly depends on various mechanisms taking place in the rock pores simultaneously. In this work, properties governing these mechanisms are presented at technically relevant conditions. The pendant and sessile drop methods are utilized to measure interfacial tension and wettability, respectively. The gravimetric method is used to quantify CO<sub>2</sub> adsorption capacity of shale and gas adsorption kinetics is evaluated to determine diffusion coefficients. It is found that interfacial properties are strongly affected by the operating pressure. The oil-CO<sub>2</sub> interfacial tension shows a decrease from approx. 21 mN/m at 0.1 MPa to around 3 mN/m at 20 MPa. A similar trend is observed in brine-CO<sub>2</sub> systems. The diffusion coefficient is observed to slightly increase with pressure at supercritical conditions. Finally, the contact angle is found to be directly related to the gas adsorption at the rock surface: Up to 3.8 wt% of CO<sub>2</sub> is adsorbed on the shale surface at 20 MPa and 60 °C where a maximum in contact angle is also found. To the best of the author's knowledge, the affinity of calcite-rich surfaces toward CO<sub>2</sub> adsorption is linked experimentally to the wetting behavior for the first time. The results are discussed in terms of CO<sub>2</sub> storage scenarios occurring optimally at 20 MPa.

**Keywords** Shale · Capillarity · Mass transport · Carbon storage · Diffusion · Interfacial tension

## Abbreviations

<i>a</i>	Radius, mm
<i>g</i>	Gravitational acceleration, m/s <sup>2</sup>
<i>n</i>	Series running index, dimensionless
<i>r</i>	Pore radius, mm
<i>t</i>	Time, minutes
<i>D</i>	Diffusion coefficient, m <sup>2</sup> /s
<i>F<sub>B</sub></i>	Buoyant force, N
<i>M/M<sub>∞</sub></i>	Mass uptake, dimensionless
<i>P</i>	Pressure, MPa

<i>P<sub>c</sub></i>	Capillary pressure, Pa
<i>T</i>	Temperature, °C
<i>V<sub>ads</sub></i>	Volume of adsorbed CO <sub>2</sub> layer, m <sup>3</sup>
<i>V<sub>s</sub></i>	Sample volume, m <sup>3</sup>
<i>θ</i>	Contact angle, °
<i>μ</i>	Viscosity, μPa.s
<i>σ<sub>lf</sub></i>	Interfacial tension between CO <sub>2</sub> and liquid (brine or oil), mN/m
<i>σ<sub>sf</sub></i>	Interfacial tension between CO <sub>2</sub> and rock surface, mN/m
<i>σ<sub>sl</sub></i>	Interfacial tension between rock surface and liquid (brine or oil), mN/m
<i>ρ<sub>ads</sub></i>	Density of adsorbed CO <sub>2</sub> phase, kg/m <sup>3</sup>
<i>ρ<sub>bulk</sub></i>	Density of bulk CO <sub>2</sub> phase, kg/m <sup>3</sup>

✉ H. Samara  
hanin.samara@tu-clausthal.de

- <sup>1</sup> Institute of Subsurface Energy Systems, Clausthal University of Technology, 38678 Clausthal-Zellerfeld, Germany
- <sup>2</sup> Eurotechnica GmbH, An den Stücken 55, 22941 Bargteheide, Germany
- <sup>3</sup> Shale Gas Research Group, Institute of Hydrocarbon Recovery, Universiti Teknologi PETRONAS, 32610 Bandar Seri Iskandar, Perak, Malaysia
- <sup>4</sup> Petroleum and Geoscience Department, Universiti Teknologi PETRONAS, 32610 Bandar Seri Iskandar, Perak, Malaysia

## Introduction

Concerns regarding anthropogenic CO<sub>2</sub> emissions are strongly growing. Tackling the increasing atmospheric CO<sub>2</sub> concentrations has become the top priority on political and environmental agendas worldwide. Carbon capture

and storage has been identified as a major technology that aims at addressing the climate change dilemma (Metz et al. 2005). It signifies a midterm mitigation strategy for the next few decades, until new energy concepts are developed on a relevant scale, for example the solar conversion of CO<sub>2</sub> into synthetic fuels (Kirsch et al. 2020). In carbon capture and storage, carbon dioxide is captured from a source of emission, purified, compressed, transported and injected into geological formations for storage (Surampalli et al. 2015). Potential geological formations for carbon storage include unminable coal seams (Ma et al. 2017), saline aquifers (Michael et al. 2009), depleted oil and gas reservoirs (Godec et al. 2011) and shales (Busch et al. 2008; Kang et al. 2011). On the other hand, the total primary energy supply has amounted to a total of approximately  $14 \times 10^6$  kilo-tons of oil equivalent in 2017 (IEA, 2017), indicating an increasing demand on energy. Due to the declining production rates of conventional reservoirs, unconventional oil and gas resources are considered potential sources of future energy (Stark et al. 2007). Despite their abundance, unconventional reservoirs are characterized by low permeability and are therefore more challenging in terms of hydrocarbon recovery (Sheng 2020). Technological advances have indeed improved the profitability of tight reservoirs by increasing the connectivity between the rock matrix and wellbore through the so-called hydraulic fracturing and horizontal drilling (Tovar et al. 2014); however, large volumes of unrecovered hydrocarbons remain trapped within the formation. Therefore, the application of enhanced oil and enhanced gas recovery technologies is still required to further improve the displacement of remaining hydrocarbons (Sheng 2015). Carbon dioxide assisted recovery technologies such as supercritical extraction (Jin et al. 2017), CO<sub>2</sub> injection either via huff and puff (Alfarge et al. 2018) or CO<sub>2</sub> flooding (Wang et al. 2010) exploit the favorable physical and chemical properties of CO<sub>2</sub> at reservoir conditions, where it commonly exists above its critical point (31.1 °C, 7.38 MPa). Supercritical CO<sub>2</sub> (sc-CO<sub>2</sub>) is characterized by high diffusivity, low viscosity and higher miscibility in crude oils relative to other gases (Lan et al. 2019) and is consequently responsible for promoting oil phase swelling (Samara and Jaeger 2021), as well as the reduction in viscosity and interfacial tension (IFT) (Perera et al. 2016), which contribute to improved displacement of residual oil that would otherwise remain unrecovered. Additionally, in unconventional organic-rich formations such as coalbeds, application of enhanced gas recovery takes advantage of the preferential adsorption of CO<sub>2</sub> on organic matter relative to CH<sub>4</sub>, which leads to the desorption of CH<sub>4</sub> and consequently enhancing methane recovery (Prusty 2008). This mechanism has also proven effective in gas shale formations (Godec et al. 2014; Tao and Clarens 2013). As a result, coupling of carbon storage with enhanced oil and gas recovery could result in the double

benefit of achieving higher hydrocarbon recovery factors and the reduction of greenhouse gases through storing CO<sub>2</sub> geologically (Liu et al. 2019).

Specific challenges arise in the case of oil and gas recovery from shales due to their extremely narrow pores, where the pore size can be in the order of nanometers (Nojabaei et al. 2013). In small confined pores, the capillary pressure is significantly large (Teklu et al. 2014) and is responsible for the entrapment of hydrocarbons within the pore space. On the other hand, due to the strong interactions of CO<sub>2</sub> with reservoir liquid and solid phases, the situation can be changed in favor of mobilizing the oil and gas trapped in these tight formations. Therefore, the fundamental parameters and prevailing mechanisms which govern fluid displacement and CO<sub>2</sub> storage need to be quantified. Several studies have investigated wettability alteration in systems comprising CO<sub>2</sub>, brines and conventional rocks (Arif et al. 2019; Mutailipu et al. 2019; Yekeen et al. 2020). However, studies involving shales are still rare in the literature. The assessment of shale wettability is either achieved through imbibition tests (Lan et al. 2015, 2014; Yassin et al. 2017) or contact angle measurements. For instance, the impact of pressure and temperature on shale wettability was investigated by (Arif et al. 2016) using the sessile drop method. They reported an increasing contact angle with increasing CO<sub>2</sub> pressure yet a reduced contact angle with increasing temperature. Shengli shale was investigated by (Pan et al. 2018). They examined the impact of pressure and salinity on the contact angle. They reported higher contact angles at higher pressures and in brines with higher salinity. In black shales (Yekeen et al. 2021) reported a decreasing contact angle at higher temperatures and an increasing contact angle in higher salinity brines and at higher pressures. Although (Shojai Kaveh et al. 2016) also reported an increasing contact angle with pressure, contrary to what had been reported earlier regarding salinity, they found lower contact angles with increasing salinities. The discrepancy in these findings may very well be attributed to the variability in mineralogy, organic matter and thermal maturity of the investigated shales which further hinders the advancement toward an undisputed understanding of shale wettability (Sharifigaliuk et al. 2021). As far as fluid–fluid interactions are concerned, several studies investigated IFT in binary systems comprising brine and CO<sub>2</sub>. The reported findings thereof are consistent and reveal a direct relation between IFT and salinity and an inverse relation between IFT and pressure. These studies are summarized in Table 1.

In spite of the aforementioned studies, a systematic work that considers all the participating phases (hydrocarbons, aqueous and solid phases), as well as their interactions, that further enables the derivation of a complete and direct picture on the situation in tight reservoirs—especially oil shales—is still lacking in the literature. This knowledge gap

**Table 1** Summary of previous studies on CO<sub>2</sub>-brine IFT

Reference	Temperature range (°C)	Pressure range (MPa)	Salinity range (wt%)	Brine composition
(Yang et al. 2005)	27 and 58	0.1–30	0.4	Saskatchewan reservoir brine
(Chiquet et al. 2007)	34–110	5–45	0 and 2	Na, Cl
(Bachu and Bennion 2009)	20–127	2–27	0–33.4	Na, K, Ca, Mg, Cl, SO <sub>4</sub> , HCO <sub>3</sub>
(Chalbaud et al. 2009)	27, 70, 100	4.5–25.5	0.5–16	Na, Cl
(Aggelopoulos et al. 2011)	27, 71, 100	5–25	0.75–25	Na, Cl, Ca
(Li et al. 2012a)	25–200	2–50	6	Na, K, Cl
(Li et al. 2012b)	70–150	2–50	4.6–55	Ca, Mg, Cl, Na, SO <sub>4</sub>
(Lun et al. 2012)	45 and 97.5	0.1–36	1.4 and 2.1	Na, Ca, Mg, Cl, SO <sub>4</sub> , HCO <sub>3</sub>
(Liu et al. 2017)	27–80	3–12	0–10.5	Na, Cl
(Mutailipu et al. 2019)	25–100	3–15	6–28	Na, K, Cl

is addressed by this work with a special focus on the utilization of CO<sub>2</sub> in oil recovery from Jordanian shale formations and their potential use for CO<sub>2</sub> storage. The first aim of the current study is to investigate fluid–fluid and rock–fluid interactions at pressures up to 40 MPa through the measurement of IFT in CO<sub>2</sub>-brine systems at conditions that have not been investigated so far, the measurement of IFT in a system comprising CO<sub>2</sub> and oil extracted from Jordanian shale, quantifying wettability alteration of the relevant system, as well as the assessment of CO<sub>2</sub> adsorption and gas diffusion. Up to the best of our knowledge, no experimental work that verifies the relation between CO<sub>2</sub> adsorption and wettability alteration of shale surfaces can be found in the literature. This experimental verification signifies the second objective of the work at hand.

## Materials

### Fluid phases

For this study, model brines of different NaCl concentrations were prepared, representing the main ions present in formation brines. The solutions were prepared by adding NaCl to deionized water at concentrations of 3 wt% and 10 wt% and stirred for 15–30 min at 300 rpm to ensure homogeneity and their complete dissolution. The monovalent ion concentrations were chosen based on the fact that they fall in the range of those that are present in unconventional reservoirs and that are relevant to carbon storage (Pan et al. 2018; Saraji et al. 2014), with the aim of assessing the impact of ion concentration on the system under investigation.

The oil phase under investigation was obtained by supercritical CO<sub>2</sub>-extraction from rocks taken from Sultani reservoir. The extraction was carried out in a laboratory-scale unit (volume 4 L, P<sub>max</sub> 69 MPa, T<sub>max</sub> 150 °C Eurotechnica, Germany) described elsewhere (Samara et al. 2019).

The extracted fluid was centrifuged for 10 min at 3000 rpm and room temperature using a centrifuge (Multifuge X1R, Thermo scientific- UK) to form two completely separate phases, one comprising the extracted formation oil and one comprising the extracted formation brine that was not further used in this study. Carbon dioxide was provided by Westfalen AG, Germany, at a purity of 99.99%.

### Solids

Shale samples were obtained from the outcrop of Al-Sultani deposit located in the central region of the Hashemite Kingdom of Jordan. For the sorption tests, a sample was cut into a nearly spherical shape with a diameter of 8.3 mm. The spherical shape facilitates the application of a mathematical approach of transient mass transfer and enables the estimation of an overall diffusion coefficient. Wetting tests were performed on a natural untreated rock sample. For the X-ray diffraction (XRD) test, powdered samples were loaded into the diffractometer with Cu K $\alpha$  radiation and a nickel filter (Empyrean—Malvern Panalytical, UK), in a 2 $\theta$  range of  $\approx$  10°–90°. Figure 1 shows the XRD pattern.

According to the XRD analysis, Sultani shale is majorly composed of calcite, followed by Quartz, Dolomite and Pyrite, which is in line with the earlier findings of (Li et al. 2019) whose tests were performed on samples taken from the same reservoir. The porosity of Sultani shale is reported by (Samara et al. 2019) to be around 20% with poor connectivity among the pores.

## Methods

### Sorption

Gas sorption on the rock surface was determined using a magnetic suspension balance (MSB) (TA instruments,

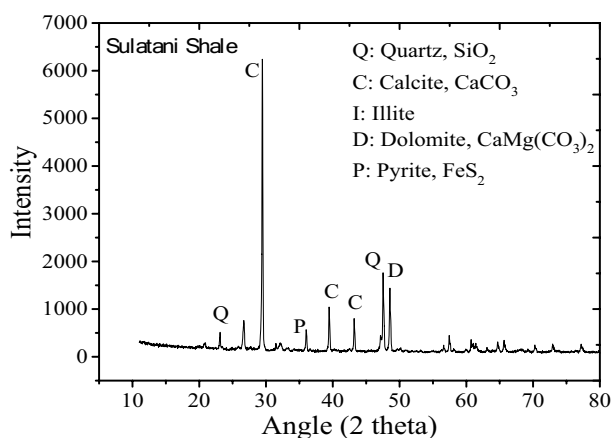


**Fig. 1** Sultani shale mineralogical composition

Germany) in a compressed CO<sub>2</sub> environment. The MSB is coupled to a high-pressure view cell by Eurotechnica GmbH ( $P_{\max}$  45 MPa,  $T_{\max}$  150 °C) that is used to observe the sample during the measurement, e.g., for any volume change taking place. The measurements are taken at 40 °C and 60 °C and a pressure range of 5 to 30 MPa. Temperature and pressure conditions are maintained constant throughout the entire sorption procedure. An electronically controlled magnetic coupling is used to transmit the weight of the sample inside the high-pressure test cell to a microbalance located outside and subject to atmospheric conditions. The sample weight is recorded as a function of time, pressure and temperature by a data acquisition software. More details on this method can be found in (Fujii et al. 2009). Upon pressurization, the sample will increase in weight over time due to gas adsorbing on the surface of the solid sample. Given the tightness of the rock, a homogeneous poreless but gas-permeable solid matter is assumed in order to enable the quantification of mass transfer by applying Fick's law of diffusion. An analytical approach that describes nonstationary diffusion of a gas into a solid sphere is provided by (Crank 1975) as per Eq. 1:

$$\left(\frac{M_t}{M_\infty}\right) = 1 - \frac{6}{n^2} \sum_{n=1}^{\infty} \frac{1}{n^2} \exp(-Dn^2\pi^2t/a^2), \quad (1)$$

where  $M_t/M_\infty$  is the mass of CO<sub>2</sub> as a function of time  $t$ ,  $n$  is the running index of the series,  $a$  is the radius of the sphere and  $D$  is the apparent diffusion coefficient. Under the assumption that the weight increase is merely the result of CO<sub>2</sub> sorption into the sample, the theoretical course of CO<sub>2</sub> mass uptake as described by Eq. 1 is adjusted by changing the apparent diffusion coefficient value until both the theoretical and experimental curves agree.

In order to remove any residual adsorbed gases and any moisture present in the solid rock, evacuation of the

high-pressure autoclave containing the sample is performed prior to pressurization. Subsequently, the autoclave is pressurized up to the designated test conditions and gas sorption begins to take place. The test is carried out until a constant value of the weight is attained.

The errors associated with measurement of CO<sub>2</sub> adsorption and diffusion coefficient are attributed to uncertainty in pressure and temperature readings, uncertainty of the starting weight signal, buoyancy effects, the extraction of soluble matter by sc-CO<sub>2</sub> and humidity. The pressure is determined by calibrated pressure sensors at a precision of  $\pm 0.2$  bar. The temperature is determined by thermocouples at a precision of  $\pm 0.1$  °C. Directly after pressurizing the autoclave, the mass measurements are subject to an error which stems from the time needed for pressure and temperature equilibration. The error associated with this phenomenon is considered the most important, where a deviation of 5% is possible, i.e., the real adsorbed CO<sub>2</sub> mass—in other words, the difference between the initial mass reading and final mass reading—could be up to 5% higher. The error resulting from buoyancy was not corrected, the reported results are those of the excess and not the absolute isotherms. Last but not least, as the sample is placed in an atmosphere of pressurized CO<sub>2</sub>, the extraction of fluids present in the sample pores by means of sc-CO<sub>2</sub> may lead to a lower apparent adsorption. To eliminate the error associated with this process, the tests are conducted on samples that have already undergone extraction prior to sorption measurements. All together the uncertainty in the sorption and diffusivity data is in the range of 1 to +6%.

## Interfacial tension

To measure the IFT of the respective fluid mixtures the pendant drop method was employed. Measurements of IFT were performed using a high-pressure view cell (PDE 1700 MD-H by Eurotechnica GmbH, Germany, wetted material (Hastelloy),  $P_{\max}$  69 MPa,  $T_{\max}$  200 °C, internal volume of 25 ml) as described in (Jaeger et al. 2010). The pendant drop method depends on drop shape adjustment when the gravity and surface forces are in equilibrium at constant T and P conditions. A calibrated thermocouple is located 10 mm from the drop inside the view cell and measures the temperature to an accuracy of  $\pm 0.1$  °C. A pressure transducer with an accuracy of  $\pm 0.1$  bar is used to measure the pressure inside the view cell. A charge-coupled device (CCD) camera records the drop shape and a drop shape analysis program-ADVANCE (Krüss GmbH, Germany)-is used to evaluate the drop profile based on the axisymmetric drop shape analysis (ADSA) technique described elsewhere (Saad and Neumann 2016). The experimental drop profile is adapted to a theoretical profile via the Young–Laplace equation which describes

the surface curvature of a liquid drop as explained in (Song and Springer 1996) by adjusting the IFT.

Determination of IFT by means of drop shape analysis requires knowledge of the densities of the participating fluid phases. The density of the oil was measured as a function of pressure and temperature using a high-pressure oscillating tube densitometer (DMA 4200 M, Anton Paar, Austria,  $P_{\max} = 50$  MPa, accuracy:  $\pm 0.2$  kg/m<sup>3</sup> and  $\pm 0.05$  °C). The density of CO<sub>2</sub> as a pure fluid is determined as a function of pressure and temperature using the GERG2008 equation of state (Kunz and Wagner 2012). Brine densities were adapted from (Liu et al. 2017) who calculated the density under similar conditions based on the empirical model developed by (Duan and Sun 2003).

A mini-dosing device with a volume of 2.5 ml is charged with the drop liquid and is connected to the view cell by means of a thin capillary. The liquid is dispensed through the thin capillary which has a diameter that allows formation of drops of appropriate shape. As previously described in (Samara et al. 2019), the tip of this capillary is located inside the view cell at the center of the two opposite pressure-resistant glass windows. After heating the view cell to the designated temperature, temperature equilibration is ensured by waiting 30 min before introducing fresh CO<sub>2</sub>. The view cell is then pressurized until the targeted pressure is reached. The cell is left again for approximately 10 to 15 min until temperature and pressure equilibration is achieved before forming a drop at the tip of the capillary. The experimental uncertainty associated with the pendant drop method may result from different factors of influence that comprise the following: errors in pressure and temperature measurement, error due to density difference between the adjacent gas and liquid phases, the uncertainty associated with the numerical analysis of the drop shape, as well as the presence of contaminants in the measurement system.

The error in determining the density difference between adjacent fluid phases is associated with the uncertainty in determining the density of the gas saturated liquid, which amounts to  $\pm 0.5\%$  in the current work. This results in an IFT measurement uncertainty in the order of  $\pm 1\%$ . Regarding the error associated with the drop shape factor, according to (Song and Springer 1996), the highest accuracy of the method is obtained at a shape factor in the range of 0.5–0.7. When the drop is too spherical, a shape factor below 0.5 is obtained and the standard deviation increases considerably. Contaminations may influence the results and lead to erroneous IFT measurements, therefore prior to IFT tests, the system was confirmed to be contaminant free by the measurement and validation of tap water IFT at atmospheric conditions ( $\sim 72$  mN/m). All in all, the mean deviation resulting from all aforementioned sources of uncertainty amounts to a maximum of  $\pm 2\%$  in the IFT range of 10–25 mN/m. Below 10 mN/m this error may increase to a value of  $\pm 5\%$  due to

larger uncertainties, especially those associated with a drop shape factor falling out of the desirable range mentioned earlier.

## Wetting

The wetting behavior was evaluated with the same setup as used in the previous sub-section. The sessile drop method is applied to determine the contact angle (CA) between the prepared brines and the surface of the rock in a compressed CO<sub>2</sub> atmosphere. As previously described in (Samara et al. 2019), these drops are recorded by a CCD camera and evaluated by the CA module of the drop shape analysis software ADVANCE (Krüss GmbH, Germany) in order to determine the three-phase CA. The error in CA measurement is mainly due to the use of a non-ideal surface as the tests were performed on natural, untreated rocks to preserve the native nature of the rocks. The images have been evaluated using different methods of drop profile approximation and CA mean values were calculated with uncertainties of  $\pm 2^\circ$ . Figure 2 shows a sessile drop of the 3 wt% NaCl brine on the Sultani rock samples.

## Results and discussion

### Oil-CO<sub>2</sub> interfacial tension

The driving force for any extraction process is the solubility of the targeted solute in the solvent. Increasing the pressure and temperature of CO<sub>2</sub> as a solvent above the critical point causes a considerable increase in its density and consequently affects its solvating power. Increasing the density of CO<sub>2</sub> translates to an increased interaction between the molecules of both the solvent and the solute, which ultimately leads to an increase in solubility (Ahmad et al. 2019).

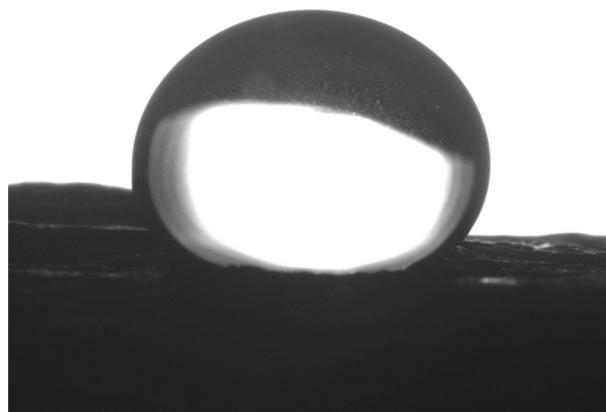


**Fig. 2** Sessile drop of 3 wt% NaCl brine on Sultani shale at 26 MPa and 60 °C



Aside from the favorable consequences of CO<sub>2</sub> dissolution into the oil such as oil swelling and viscosity reduction (Li et al. 2013), its impact on interfacial tension (IFT) is relevant for mobilizing the oil and increasing its recovery. Interfacial tension is related to the capillarity pressure ( $P_c$ ) within the pores via the Young–Laplace Eq. 2 (Arif et al. 2016):

$$P_c = \frac{2\sigma_{lf}}{r} \cdot \cos\theta, \quad (2)$$

where  $\sigma_{lf}$  is the IFT between the reservoir liquid and CO<sub>2</sub>,  $\theta$  is the CA between the fluid interface and the rock at the three-phase contact point and  $r$  is the pore radius. Therefore, a reduction in the IFT results in reducing the capillary pressure and consequently an increase in oil recovery. The oil–CO<sub>2</sub> IFT at 60 °C is shown in Fig. 3.

At low to moderate pressures, the IFT course is dominated by the interaction of CO<sub>2</sub> with the light compounds of the crude oil, this is indicated by a steep slope that is qualitatively similar to that observed for a gas condensate/CO<sub>2</sub> system as reported in (Wang et al. 2019), where complete miscibility is reached at moderate pressures below 15 MPa. This can be attributed to the reduction in the intermolecular distance between CO<sub>2</sub> and the oil as pressure increases, thereby increasing the intermolecular forces between them (Yang et al. 2015). Additionally, this signifies increased solubility of CO<sub>2</sub> in the oil and consequently a reduced IFT (Hemmati-Sarapardeh et al. 2014; Rezk and Foroozesh 2019). On the other hand, the leveling off of the curve at high pressure (around 14 MPa) shows a typical IFT course that signifies the presence of heavier components. This is in line with the findings of (Yang and Gu 2005; Yang et al. 2015). The heavier fractions of oil exhibit less mutual solubility with CO<sub>2</sub> (Marufuzzaman and Henni 2015) and

therefore a considerable reduction in IFT can no longer be observed.

### Brine–CO<sub>2</sub> interfacial tension

In order to understand the phase behavior between injected CO<sub>2</sub> and formation brine, the IFT of a binary system comprising CO<sub>2</sub> and model brines has been investigated. Figure 4 shows the IFT between CO<sub>2</sub> and two different brines (3 wt% and 10 wt% NaCl) at 60 °C.

It is observed that the IFT decreases as pressure increases for both NaCl concentrations. At pressures up to 20 MPa, the decrease in IFT is significant. This is attributed to the fact that as pressure increases, CO<sub>2</sub> solubility in brine considerably increases at low to moderate pressures (Duan et al. 2006; Duan and Sun 2003). On the other hand, at elevated pressures the slope of IFT reduction decreases until a further drop in IFT is hardly observable. At higher pressures, CO<sub>2</sub> becomes increasingly incompressible and the influence of pressure on CO<sub>2</sub> density declines ( $\Delta\rho/\Delta P$  is reduced). This in turn influences the solubility of CO<sub>2</sub> in the brine and explains why the IFT curves level off (Mosavat et al. 2014). It is worth mentioning that the pressure at which constant IFT values are observed is independent of the brine salinity, which is in line with the work of (Chalbaud et al. 2009). Their findings could also be confirmed in terms of the influence of the salinity: Fig. 4 shows that the isobaric IFT is also higher for the brine with the higher salinity. This is explained by the spatial distribution of monovalent ions (Na<sup>+</sup>) in the aqueous phase and its impact on the interfacial configuration of water molecules (Aggelopoulos et al. 2011). Cations have no affinity to the liquid–gas interface and are therefore repelled from the respective front, consequently accumulating in the aqueous solution. As a result, water

**Fig. 3** Interfacial tension between extracted oil and CO<sub>2</sub> as a function of pressure at 60 °C

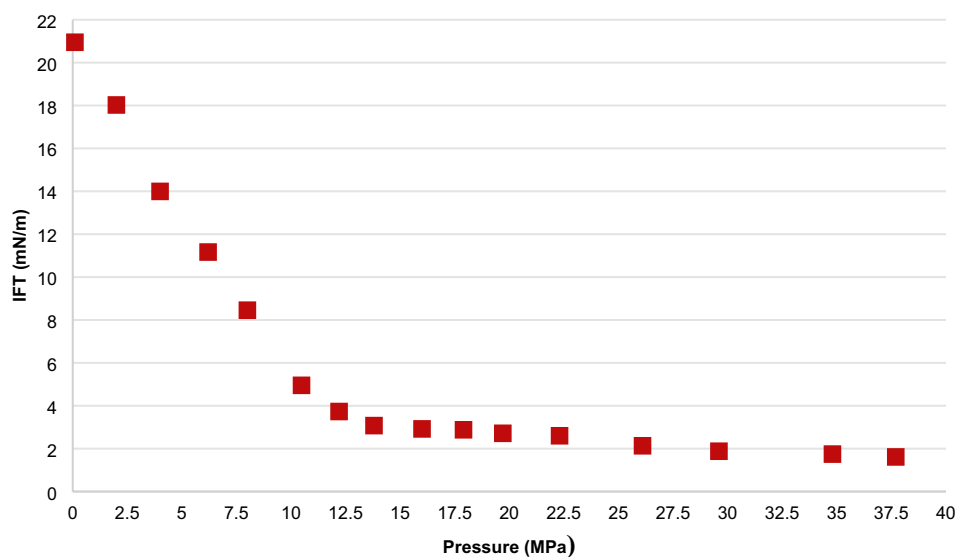
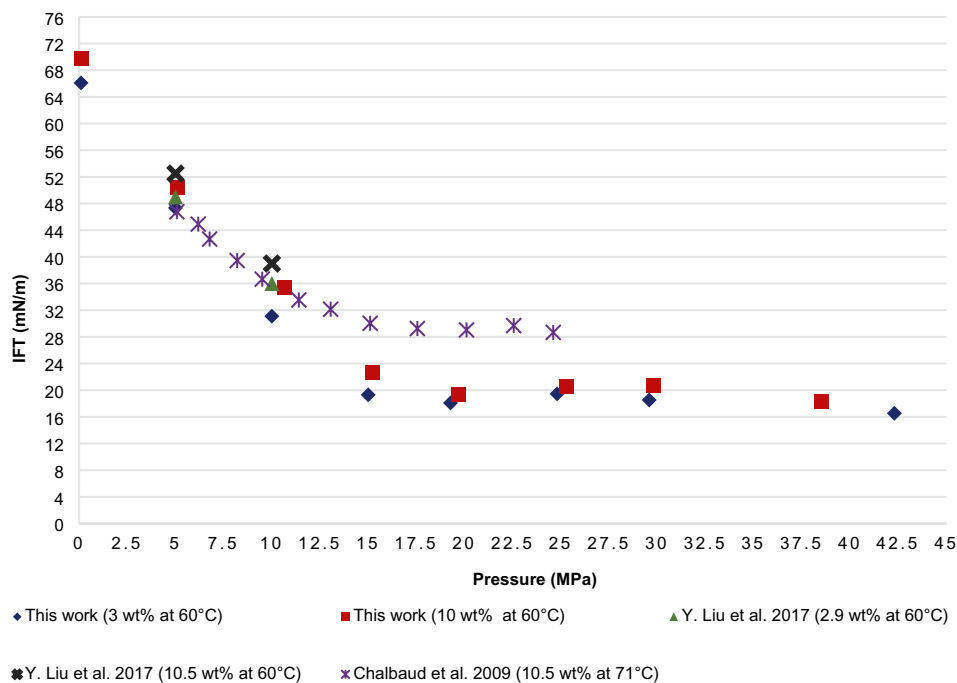


**Fig. 4** CO<sub>2</sub>-NaCl brine interfacial tension as a function of pressure and salinity at 60 °C. For comparison, literature data are also plotted (Chalbaud et al. 2009), (Liu et al. 2017))



molecules located at the interface migrate toward the aqueous bulk phase to solvate the cations in what is also known as ion hydration (Chalbaud et al. 2009; Levin and Flores-Mena 2001), and therefore the number of water molecules available to interact with the CO<sub>2</sub> is reduced (Mirchi et al. 2014). This results in a reduction of mutual solubility and accordingly a higher CO<sub>2</sub>-brine IFT is observed for brines with higher salt concentration (Bachu and Bennion 2009).

The brine concentration in this study is almost similar to that investigated by (Chalbaud et al. 2009) (10.5 wt%), the reported values there show lower IFT at low pressures due to the higher temperature (71 °C). Conversely, as the pressure increases beyond 10 MPa, IFT undergoes an inversion and is higher at higher temperature, which is a known phenomenon (Chalbaud et al. 2009; Li et al. 2012a) and is also related to the density behavior of CO<sub>2</sub>. Brines with similar concentrations were investigated by (Liu et al. 2017) at 60 °C; however, only two IFT measurements are reported for each brine, which makes it difficult to evaluate and explain the existing discrepancy. On the other hand, IFT measurements reported in this work are consistent among each other. A more comprehensive comparison to previously published values is not possible because IFT measurements at high pressures are lacking in the literature for brines with similar salinity at 60 °C.

## Sorption

Sorption measurements have been successively conducted on the same sample described in the materials section. The sample had already undergone extraction in order to

minimize any interference by fluids originally present in the rock such as oil or formation brine which occupy the pore space, consequently reducing the surface area available for the CO<sub>2</sub> to adsorb (Rani et al. 2019). The sorption kinetics of CO<sub>2</sub> on Sultani shale is exemplarily depicted in Fig. 5. Sorption kinetics are used to determine the adsorption capacity of the shale as per Eq. 1 in the methods section. After a strong initial increase, the adsorbed CO<sub>2</sub> mass reaches equilibrium at around 200 min. Figure 6 shows the adsorption capacity of CO<sub>2</sub> as wt% of the rock at two temperatures (40 °C and 60 °C) as a function of pressure as well as the bulk densities of CO<sub>2</sub> as calculated by GERG2008 equation of state (Kunz and Wagner 2012).

At a constant temperature, the adsorption isotherms show a strong increase in adsorption capacity near the critical state of CO<sub>2</sub>. This increase is related to the sharp increase in CO<sub>2</sub> density as it changes from the gaseous state to the supercritical state (Klewiah et al. 2020). However, this increase is only observed until a certain pressure is reached. For both investigated temperatures, the adsorption capacity peaks at 20 MPa with no significant difference over values measured at 15 MPa: In the gravimetric sorption measurement method, the net increase in mass uptake is a superposition of two forces; the adsorption of gas molecules on the adsorbent (positive), and the buoyancy force that acts against the latter (negative) (Gasparik et al. 2014). The buoyancy force is given in Eq. 3 (Abdul Kareem et al. 2018):

$$F_B = V_s \cdot \rho_{\text{bulk}} \cdot g, \quad (3)$$

**Fig. 5** CO<sub>2</sub> adsorption kinetics on Sultani shale at 15 MPa and 40 °C

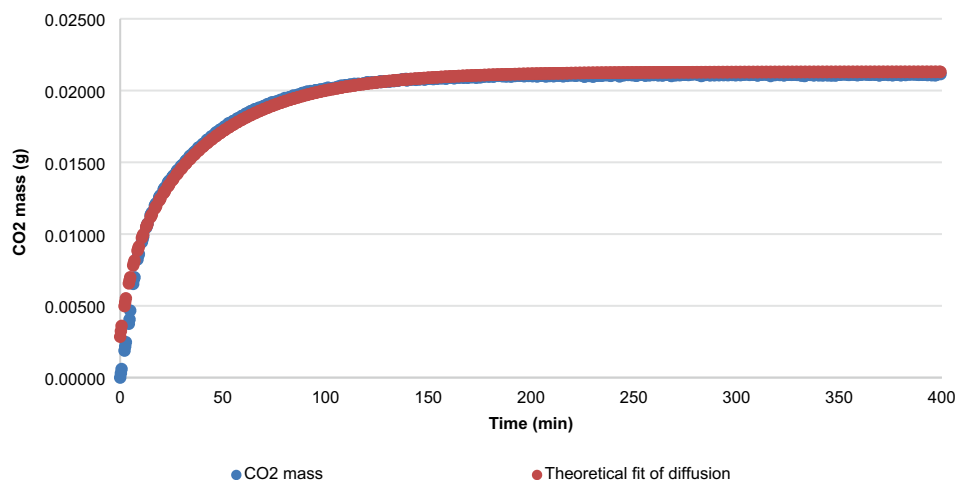
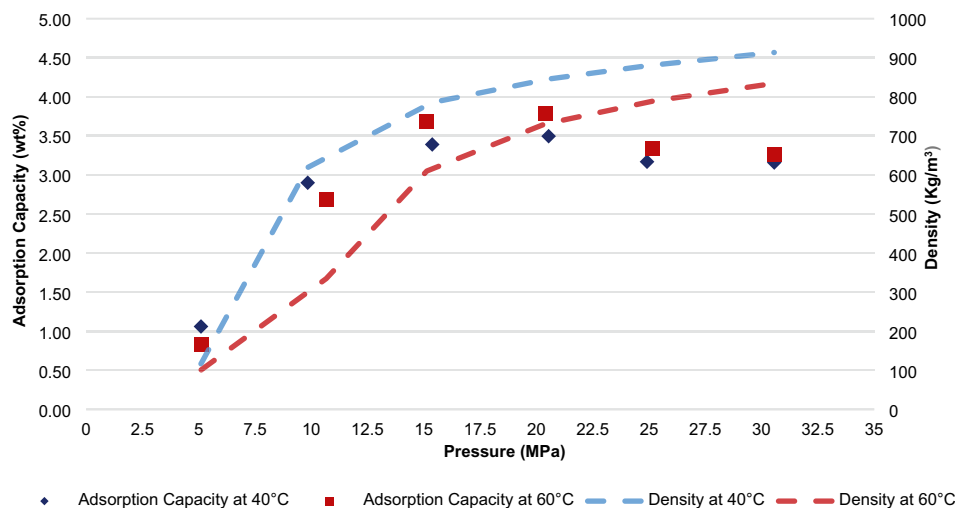


**Fig. 6** Density of bulk phase CO<sub>2</sub> and CO<sub>2</sub> adsorption capacity of Sultani shale as a function of pressure at 40 °C and 60 °C



where  $F_B$  is the buoyant force,  $V_s$  is the sample volume,  $\rho_{bulk}$  is the density of bulk CO<sub>2</sub> and  $g$  is the gravitational acceleration. At lower pressures, the density of the bulk phase ( $\rho_{bulk}$ ) is low and therefore the buoyant force acting upward on the sample can be neglected. However, as the pressure increases,  $\rho_{bulk}$  increases, consequently increasing the buoyant force and the excess adsorption isotherm appears to be lower (Fujii et al. 2010), which occurs beyond 20 MPa.

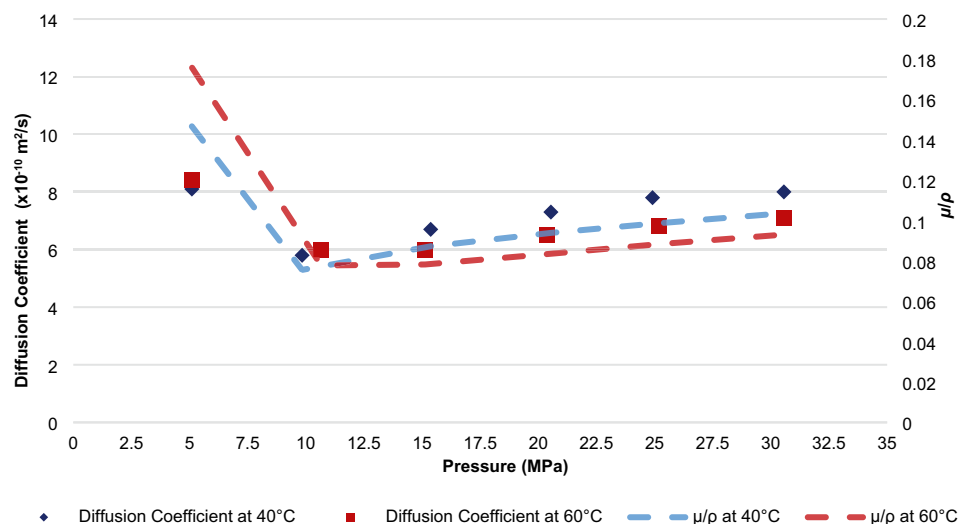
On the other hand, at low pressure the adsorption capacities at 40 °C is higher than 60 °C. Conversely, as the pressure increases, the adsorption capacity at 60 °C appears to be higher. This can also be justified by the buoyancy effect as follows: At high pressure the occupancy of sorption sites by the adsorbed molecules is already high, and therefore it may be assumed that the density of the adsorbed phase does not increase much with pressure and the volume of adsorbed phase remains relatively constant. Consequently, the density of bulk CO<sub>2</sub> determines the magnitude of change in buoyancy forces interfering with the adsorption capacity. From Fig. 6, it is observed that  $\rho_{bulk}$  at 40 °C is higher than

that for 60 °C. This implies that the effect of buoyancy forces on the sample is higher at 40 °C than 60 °C and increases at higher pressure. As a result, the buoyancy-induced error on the 40 °C adsorption isotherm is larger compared to the 60 °C isotherm. Therefore, excess isotherm correction would yield higher absolute adsorption isotherms for 40 °C. This is in line with what was stated in ref (Fujii et al. 2010), who reported a higher buoyancy effect at 50 °C compared to 100 °C. However, the conversion of the excess isotherm to an absolute isotherm with buoyancy correction cannot be determined as neither the exact volume of adsorbed CO<sub>2</sub> ( $V_{ads}$ )—which increases the volume of the sample—nor the density of the adsorbed CO<sub>2</sub> layer ( $\rho_{ads}$ ) can be measured.

Figure 7 depicts the apparent diffusion coefficients ( $D$ ) as estimated using Eq. 1. The results show that as CO<sub>2</sub> transitions from the gaseous state into the supercritical state, the diffusion coefficient is reduced. Additionally, it is also observed that the dominating diffusion mechanism is self-diffusion, since the experimental values qualitatively follow the first approximation of the rigid sphere model as



**Fig. 7** CO<sub>2</sub> diffusion coefficient as a function of pressure at 40 °C and 60 °C



described by Chapman and Cowling in (Jost 1952). This model estimates the coefficient of self-diffusion and is given in Eq. 4:

$$D_{11} = 1.2 \frac{\mu}{\rho}, \quad (4)$$

where  $\mu$  and  $\rho$  are the gas dynamic viscosity and density, respectively, at given pressure and temperature conditions. This therefore implies that the diffusion—unlike surface diffusion and Knudsen diffusion—is independent of the pore diameter.

It can also be observed that while at 5 MPa the coefficient is higher for the higher temperature; the opposite is observed at higher pressures. However, at both temperatures, the diffusion coefficient is observed to slightly increase with increasing pressure at supercritical conditions. Following Eq. 4 and in accordance with the experimental findings, the dynamic viscosity at lower temperature (40 °C) is the dominating effect at higher pressures for which it may be inferred that friction between molecules of the same type enhances diffusion whereas it is well known that in binary diffusion the opposite occurs.

### Wettability analysis

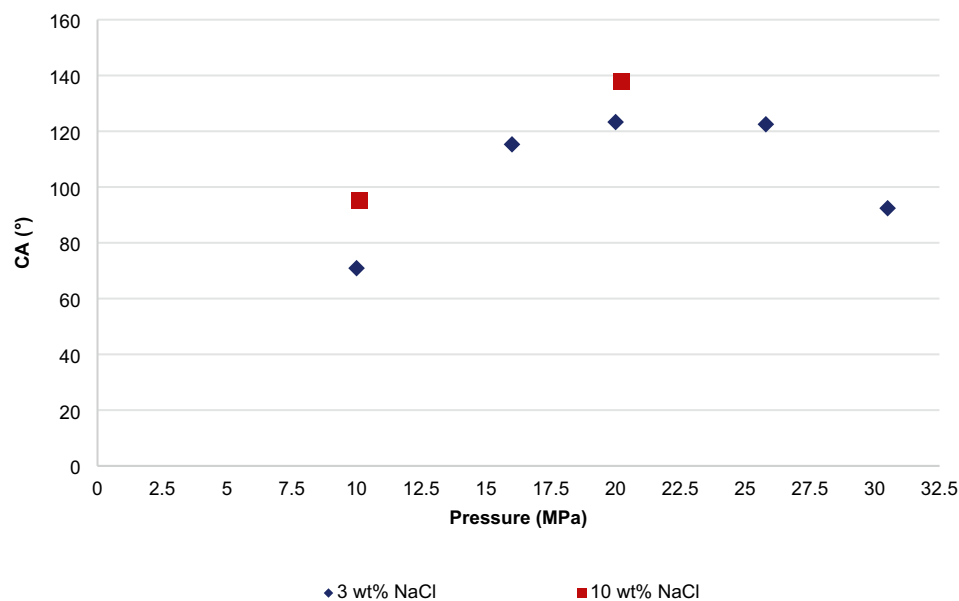
Wettability of a fluid-rock system affects the distribution and flow of fluids within the reservoir. It signifies the preferential affinity of the rock toward one of the fluids present in the reservoir. Wetting is correlated with the capillary pressure ( $P_c$ ) by means of the contact angle (CA),  $\theta$  and the interfacial tension  $\delta_{if}$  in Eq. 2. Young's equation correlates the CA to the IFT between the different phases comprising a reservoir system and is presented in Eq. 5 (Shojai Kaveh et al. 2016):

$$\cos \theta = \frac{6s_f - 6s_l}{6lf}, \quad (5)$$

where  $\delta_{sf}$  is the IFT between the solid and CO<sub>2</sub>,  $\delta_{sl}$  is the IFT between the solid and liquid (brine),  $\delta_{lf}$  is the IFT between reservoir liquid (brine) and CO<sub>2</sub> and  $\theta$  is the CA at the point of three-phase contact. In the literature, several classifications of wetting behavior exist in terms of CA values like those reported in (Fanchi 2018; Schön 2011). Those reported in (Schön 2011) are considered here, where rock surfaces are classified into water wet when  $0^\circ < \theta < 70^\circ$ , intermediate wet when  $70^\circ < \theta < 110^\circ$ , and oil wet when  $110^\circ < \theta < 180^\circ$ . In the context of this study, the wetting of the reservoir rock by model brines in the presence of CO<sub>2</sub> is investigated as shown in Fig. 8.

For the 3 wt% NaCl brine, it is observed that the CA is an increasing function of pressure. This is, however, only valid for moderate pressures ranging between 10 and 20 MPa. At higher pressures, the CA decreases with increasing pressure. This can be attributed to the following: The CA is the result of the superposition of IFT between CO<sub>2</sub>, brine and rock as indicated by Eq. 5 (Espinoza and Santamarina 2010). By examining Fig. 6, it can be seen that the adsorption capacity of CO<sub>2</sub> on the rock surface increases until a pressure of 20 MPa is reached, beyond which the adsorption capacity declines. The adsorption of CO<sub>2</sub> molecules on the rock surface reduces the IFT between CO<sub>2</sub> and the rock surface ( $\delta_{sf}$ ) and results in a higher CA according to Eq. 5. Figure 4 shows that the IFT between the CO<sub>2</sub> and the brine ( $\delta_{lf}$ ) decreases until 20 MPa is reached. Referring back to Eq. 5, this would imply a reduction in the CA, however, that is not the case; therefore, it can be assumed that the effect of  $\delta_{sf}$  is more pronounced than that of  $\delta_{lf}$  in determining CA. Beyond 20 MPa,  $\delta_{sf}$  decreases but  $\delta_{lf}$  is relatively constant and therefore a reduction in CA is observed. All of this explains the

**Fig. 8** Contact angle measurement of brines on Al-Sultani shale in a CO<sub>2</sub> atmosphere at 60 °C



transition of rock wettability from being intermediate wet at 10 MPa to being CO<sub>2</sub> wet for the range of 16 to 26 MPa and the reversal of wettability again at 30 MPa (intermediate wet). This behavior is in line with the findings reported by (Arif et al. 2017; Shojai Kaveh et al. 2016) where it was observed that increasing the pressure makes the system more CO<sub>2</sub> wet.

From a general point of view, brine salinity does not seem to impact the wettability as the rock is classified as intermediate wet at 10 MPa and CO<sub>2</sub> wet at 20 MPa with both brines. However, the difference in CA measurements could be explained as follows: Examining Fig. 4 and Eq. 5 once again, it can be seen that a higher  $\sigma_{if}$  increases the CA ( $\sigma_{if, 10\text{ wt}\%} > \sigma_{if, 3\text{ wt}\%}$ ), which explains why the brine with the higher salinity exhibits higher CA at the respective pressures. This is also in line with the findings of (Arif et al. 2017) who measured CA and similarly showed an increasing CA for higher salinity brines on calcite, which is a major constituent of Al-Sultani shale as confirmed by the XRD results.

## Conclusion

In the current study, the phase behavior and mutual interactions of binary and ternary fluid–solid systems have been investigated in view of their significance for oil extraction and CO<sub>2</sub> storage. A series of tests have been conducted to assess the CO<sub>2</sub> adsorption capacity of the rock, the CO<sub>2</sub>-oil and CO<sub>2</sub>-brine IFT along with the wettability of the rock surface at elevated pressures. In line with previous findings, the CO<sub>2</sub>-brine and CO<sub>2</sub>-oil IFT decrease as a function of pressure as mutual solubility is enhanced.

The results also indicate that the CO<sub>2</sub>-oil IFT reaches a semi-plateau at 15 MPa beyond which no further reduction is observed. This implies that oil recovery will not be drastically enhanced when pressures higher than 15 MPa are applied. The CO<sub>2</sub>-brine IFT plateau also implies that the storage of CO<sub>2</sub> at pressures higher than 20 MPa will not promote the dissolution of higher amounts of CO<sub>2</sub> into the reservoir brine. Additionally, the IFT is observed to be an increasing function of salinity, which suggests that reservoirs with low salinity brines are more suitable for the application of carbon storage due to enhanced solubility trapping. This is also implied by the higher water wetting of low salinity brine, which promotes better capillary trapping of CO<sub>2</sub> as a residual discontinuous phase below the brine.

Measurements of CA also reveal that water wetting decreases with increased pressure until an inversion occurs beyond 20 MPa, which is consistent with the adsorption tests that reveal a maximum adsorption capacity at 20 MPa, beyond which the excess adsorption isotherms drop, suggesting that this is the decisive property to explain the maximum in CA. Further, the diffusion coefficient is observed to qualitatively follow the rigid sphere model which estimates the coefficient of self-diffusion, implying that self-diffusion is the dominating mechanism in the process of mass transfer. As a general conclusion, it may be stated that increasing the pressure up to 20 MPa has mainly positive effects on oil mobility as well as CO<sub>2</sub> storage capacity, which also takes its maximum value at the respective pressure where it may be inferred that the amount of stored CO<sub>2</sub> via the so-called solubility and adsorption trapping mechanisms is maximized, indicating optimum process conditions of 20 MPa while the temperature interestingly exhibits only little influence.

**Acknowledgements** We acknowledge financial support by the Open Access Publishing Fund of Clausthal University of Technology.

**Funding** Open Access funding enabled and organized by Projekt DEAL. This research received no specific grant from any funding agency in the public, commercial, or not-for-profit sectors.

## Declarations

**Conflict of interest** The authors declare no competing financial or non-financial interests.

**Open Access** This article is licensed under a Creative Commons Attribution 4.0 International License, which permits use, sharing, adaptation, distribution and reproduction in any medium or format, as long as you give appropriate credit to the original author(s) and the source, provide a link to the Creative Commons licence, and indicate if changes were made. The images or other third party material in this article are included in the article's Creative Commons licence, unless indicated otherwise in a credit line to the material. If material is not included in the article's Creative Commons licence and your intended use is not permitted by statutory regulation or exceeds the permitted use, you will need to obtain permission directly from the copyright holder. To view a copy of this licence, visit <http://creativecommons.org/licenses/by/4.0/>.

## References

- Abdul Kareem FA, Shariff AM, Ullah S, Dreisbach F, Keong LK, Melion N, Garg S (2018) Experimental measurements and modeling of supercritical CO<sub>2</sub> adsorption on 13X and 5A zeolites. *J Nat Gas Sci Eng* 50:115–127. <https://doi.org/10.1016/j.jngse.2017.11.016>
- Aggelopoulos CA, Robin M, Vizika O (2011) Interfacial tension between CO<sub>2</sub> and brine (NaCl+CaCl<sub>2</sub>) at elevated pressures and temperatures: the additive effect of different salts. *Adv Water Resour* 34:505–511. <https://doi.org/10.1016/j.advwatres.2011.01.007>
- Ahmad T, Masoodi FA, Rather SA, Wani SM, Gull A (2019) Supercritical fluid extraction: a review. *J. Biol. Chem. Chron.* 5:114–122. <https://doi.org/10.33980/jbcc.2019.v05i01.019>
- Alfarge D, Wei M, Bai B (2018) CO<sub>2</sub>-EOR mechanisms in huff-n-puff operations in shale oil reservoirs based on history matching results. *Fuel* 226:112–120. <https://doi.org/10.1016/j.fuel.2018.04.012>
- Arif M, Al-Yaseri AZ, Barifceni A, Lebedev M, Iglauer S (2016) Impact of pressure and temperature on CO<sub>2</sub>-brine-mica contact angles and CO<sub>2</sub>-brine interfacial tension: implications for carbon geo-sequestration. *J Colloid Interface Sci* 462:208–215. <https://doi.org/10.1016/j.jcis.2015.09.076>
- Arif M, Lebedev M, Barifceni A, Iglauer S (2017) CO<sub>2</sub> storage in carbonates: wettability of calcite. *Int J Greenh Gas Control* 62:113–121. <https://doi.org/10.1016/j.ijggc.2017.04.014>
- Arif M, Abu-Khamsin SA, Iglauer S (2019) Wettability of rock/CO<sub>2</sub>/brine and rock/oil/CO<sub>2</sub>-enriched-brine systems: critical parametric analysis and future outlook. *Adv Colloid Interface Sci* 268:91–113. <https://doi.org/10.1016/j.cis.2019.03.009>
- Bachu S, Bennion DB (2009) Interfacial tension between CO<sub>2</sub>, freshwater, and brine in the range of pressure from (2 to 27) MPa, temperature from (20 to 125)°C, and water salinity from (0 to 334 000) mg·L<sup>-1</sup>. *J Chem Eng Data* 54:765–775. <https://doi.org/10.1021/je800529x>
- Busch A, Alles S, Gensterblum Y, Prinz D, Dewhurst D, Raven M, Stanjek H, Krooss B (2008) Carbon dioxide storage potential of shales. *Int J Greenh Gas Control* 2:297–308. <https://doi.org/10.1016/j.ijggc.2008.03.003>
- Chalabaud C, Robin M, Lombard J-M, Martin F, Egermann P, Bertin H (2009) Interfacial tension measurements and wettability evaluation for geological CO<sub>2</sub> storage. *Adv Water Resour* 32:98–109. <https://doi.org/10.1016/j.advwatres.2008.10.012>
- Chiquet P, Daridon J-L, Broseta D, Thibeau S (2007) CO<sub>2</sub>/water interfacial tensions under pressure and temperature conditions of CO<sub>2</sub> geological storage. *Energy Convers Manag* 48:736–744. <https://doi.org/10.1016/j.enconman.2006.09.011>
- Crank J (1975) *The mathematics of diffusion*, 2d edn. Clarendon Press, Oxford ([Eng])
- Duan Z, Sun R (2003) An improved model calculating CO<sub>2</sub> solubility in pure water and aqueous NaCl solutions from 273 to 533 K and from 0 to 2000 bar. *Chem Geol* 193:257–271. [https://doi.org/10.1016/S0009-2541\(02\)00263-2](https://doi.org/10.1016/S0009-2541(02)00263-2)
- Duan Z, Sun R, Zhu C, Chou I-M (2006) An improved model for the calculation of CO<sub>2</sub> solubility in aqueous solutions containing Na<sup>+</sup>, K<sup>+</sup>, Ca<sup>2+</sup>, Mg<sup>2+</sup>, Cl<sup>-</sup>, and SO<sub>4</sub><sup>2-</sup>. *Mar Chem* 98:131–139. <https://doi.org/10.1016/j.marchem.2005.09.001>
- Espinoza DN, Santamarina JC (2010) Interfacial tension, contact angle, and diffusion-Implications to CO<sub>2</sub> geological storage: water CO<sub>2</sub> Mineral Systems. *Water Resour Res.* <https://doi.org/10.1029/2009WR008634>
- Fanchi, JR (2018) Chapter 5—Rock–Fluid Interaction, in: Fanchi, J.R. (Ed.), *Principles of applied reservoir simulation* (Fourth Edition). Gulf Professional Publishing, pp. 81–99. <https://doi.org/10.1016/B978-0-12-815563-9.00005-7>
- Fujii T, Sato Y, Lin H, Inomata H, Hashida T (2009) Evaluation of CO<sub>2</sub> sorption capacity of rocks using a gravimetric method for CO<sub>2</sub> geological sequestration. *Energy Procedia* 1:3723–3730. <https://doi.org/10.1016/j.egypro.2009.02.171>
- Fujii T, Nakagawa S, Sato Y, Inomata H, Hashida T (2010) Sorption characteristics of CO<sub>2</sub> on rocks and minerals in storing CO<sub>2</sub> processes. *Nat Resour* 01:1–10. <https://doi.org/10.4236/nr.2010.11001>
- Gasparik M, Rexer TFT, Aplin AC, Billemont P, De Weireld G, Gensterblum Y, Henry M, Krooss BM, Liu S, Ma X, Sakurovs R, Song Z, Staib G, Thomas KM, Wang S, Zhang T (2014) First international inter-laboratory comparison of high-pressure CH<sub>4</sub>, CO<sub>2</sub> and C<sub>2</sub>H<sub>6</sub> sorption isotherms on carbonaceous shales. *Int J Coal Geol* 132:131–146. <https://doi.org/10.1016/j.coal.2014.07.010>
- Godec M, Koperna G, Petrusak R, Oudinot A (2014) Enhanced gas recovery and CO<sub>2</sub> storage in gas shales: a summary review of its status and potential. *Energy Procedia* 63:5849–5857. <https://doi.org/10.1016/j.egypro.2014.11.618>
- Godec M, Kuuskraa V, Van Leeuwen T, Stephen Melzer L, Wildgust N, (2011) CO<sub>2</sub> storage in depleted oil fields: The worldwide potential for carbon dioxide enhanced oil recovery. *Energy Procedia*, 10th International conference on greenhouse gas control technologies 4, 2162–2169. <https://doi.org/10.1016/j.egypro.2011.02.102>
- Hemmati-Sarapardeh A, Ayatollahi S, Ghazanfari M-H, Masihi M (2014) Experimental determination of interfacial tension and miscibility of the CO<sub>2</sub>-Crude oil system: temperature, pressure, and composition effects. *J Chem Eng Data* 59:61–69. <https://doi.org/10.1021/je400811h>
- International Energy Agency (IEA), (2017) *Data and Statistics*. <https://www.iea.org/data-and-statistics/data-tables/?country=WORLD&energy=Balances&year=2017>
- Jaeger PT, Alotaibi MB, Nasr-El-Din HA (2010) Influence of compressed carbon dioxide on the capillarity of the gas-crude oil-reservoir water system. *J Chem Eng Data* 55:5246–5251. <https://doi.org/10.1021/je100825b>

- Jin L, Hawthorne S, Sorensen J, Pekot L, Kurz B, Smith S, Heebink L, Bosshart N, Torres J, Dalkhaa C, Gorecki C, Steadman E, Harju J (2017) Extraction of Oil from the Bakken Shales with Supercritical CO<sub>2</sub>. In: Proceedings of the 5th Unconventional Resources Technology Conference. American Association of Petroleum Geologists, Austin, Texas, USA. <https://doi.org/10.15530/URTEC-2017-2671596>
- Jost W (1952) Diffusion in solids, liquids, Gases. Academic Press, New York
- Kang SM, Fathi E, Ambrose RJ, Akkutlu IY, Sigal RF (2011) Carbon dioxide storage capacity of organic-rich shales. Soc Pet Eng. <https://doi.org/10.2118/134583-PA>
- Kirsch H, Brübach L, Loewert M, Riedinger M, Gräfenhahn A, Böltken T, Klumpp M, Pfeifer P, Dittmeyer R (2020) CO<sub>2</sub>-neutrale Fischer-Tropsch-Kraftstoffe aus dezentralen modularen Anlagen: status und Perspektiven. Chem Ing Tech 92:91–99. <https://doi.org/10.1002/cite.201900120>
- Klewiah I, Berawala DS, Alexander Walker HC, Andersen PØ, Nadeau PH (2020) Review of experimental sorption studies of CO<sub>2</sub> and CH<sub>4</sub> in shales. J Nat Gas Sci Eng 73:103045. <https://doi.org/10.1016/j.jngse.2019.103045>
- Kunz O, Wagner W (2012) The GERG-2008 wide-range equation of state for natural gases and other mixtures: an expansion of GERG-2004. J Chem Eng Data 57:3032–3091. <https://doi.org/10.1021/jc300655b>
- Lan Q, Xu M, Binazadeh M, Dehghanpour H, Wood JM (2015) A comparative investigation of shale wettability: the significance of pore connectivity. J Nat Gas Sci Eng 27:1174–1188. <https://doi.org/10.1016/j.jngse.2015.09.064>
- Lan Y, Yang Z, Wang P, Yan Y, Zhang L, Ran J (2019) A review of microscopic seepage mechanism for shale gas extracted by supercritical CO<sub>2</sub> flooding. Fuel 238:412–424. <https://doi.org/10.1016/j.fuel.2018.10.130>
- Lan, Q., Xu, M., Dehghanpour, H., Wood, J., (2014) Advances in Understanding Wettability of Tight and Shale Gas Formations, In: SPE Annual Technical Conference and Exhibition. Presented at the SPE Annual Technical Conference and Exhibition, Society of Petroleum Engineers, Amsterdam, The Netherlands. <https://doi.org/10.2118/170969-MS>
- Levin Y, Flores-Mena JE (2001) Surface tension of strong electrolytes. Europhys Lett 56:7
- Li X, Boek E, Maitland GC, Trusler JPM (2012a) Interfacial tension of (Brines + CO<sub>2</sub>): (0.864 NaCl + 0.136 KCl) at temperatures between (298 and 448) K, pressures between (2 and 50) MPa, and total molalities of (1 to 5) mol·kg<sup>-1</sup>. J Chem Eng Data 57:1078–1088. <https://doi.org/10.1021/jc201062r>
- Li X, Boek ES, Maitland GC, Trusler JPM (2012b) Interfacial Tension of (Brines + CO<sub>2</sub>): CaCl<sub>2</sub> (aq), MgCl<sub>2</sub> (aq), and Na<sub>2</sub>SO<sub>4</sub> (aq) at Temperatures between (343 and 423) K, Pressures between (2 and 50) MPa, and Molalities of (0.5 to 5) mol·kg<sup>-1</sup>. J Chem Eng Data 57:1369–1375. <https://doi.org/10.1021/jc300304p>
- Li H, Zheng S, Yang D (2013) Enhanced swelling effect and viscosity reduction of Solvent(s)/CO<sub>2</sub>/Heavy-Oil Systems. SPE J. 13
- Li K, Samara H, Wang X, Jaeger P, Ganzer L, Wegner J, Xie L (2019) Reservoir characteristics and resource potential of oil shale in Sultani Area, Central of Jordan, in: Abu Dhabi international petroleum exhibition and conference. Presented at the Abu Dhabi International Petroleum Exhibition and Conference, Society of Petroleum Engineers, Abu Dhabi, UAE. <https://doi.org/10.2118/197606-MS>
- Liu Y, Tang J, Wang M, Wang Q, Tong J, Zhao J, Song Y (2017) Measurement of interfacial tension of CO<sub>2</sub> and NaCl aqueous solution over wide temperature, pressure, and salinity ranges. J Chem Eng Data 62:1036–1046. <https://doi.org/10.1021/acs.jced.6b00858>
- Liu D, Li Y, Yang S, Agarwal RK (2019) CO<sub>2</sub> sequestration with enhanced shale gas recovery. Energy Sources Part Recovery Util. Environ Eff. <https://doi.org/10.1080/15567036.2019.1587069>
- Lun Z, Fan H, Wang H, Luo M, Pan W, Wang R (2012) Interfacial tensions between reservoir brine and CO<sub>2</sub> at high pressures for different salinity. Energy Fuels 26:3958–3962. <https://doi.org/10.1021/ef300440w>
- Ma T, Rutqvist J, Liu W, Zhu L, Kim K (2017) Modeling of CO<sub>2</sub> sequestration in coal seams: role of CO<sub>2</sub>-induced coal softening on injectivity, storage efficiency and caprock deformation. Greenh Gases Sci Technol 7:562–578. <https://doi.org/10.1002/ghg.1664>
- Marufuzzaman M, Henni A (2015) Solubility of CO<sub>2</sub> and C<sub>2</sub>H<sub>6</sub> in Heavy Oil and its Sara Fractions. Can J Chem Eng 93:553–564. <https://doi.org/10.1002/cjce.22150>
- Metz B, Davidson O, de Coninck H, Loos M, Meyer L (2005) IPCC special report on carbon dioxide capture and storage. Cambridge University Press
- Michael K, Arnot M, Cook P, Ennis-King J, Funnell R, Kaldi J, Kirste D, Paterson L (2009) CO<sub>2</sub> storage in saline aquifers I—Current state of scientific knowledge. Energy Procedia, Greenhouse Gas Control Technologies 9(1):3197–3204. <https://doi.org/10.1016/j.egypro.2009.02.103>
- Mirchi V, Saraji S, Goual L, Piri M (2014) Dynamic interfacial tensions and contact angles of Surfactant-in-Brine/Oil/Shale Systems: implications to enhanced oil recovery in shale oil reservoirs, in: SPE improved oil recovery symposium. Presented at the SPE Improved Oil Recovery Symposium, Society of Petroleum Engineers, Tulsa, Oklahoma, USA. <https://doi.org/10.2118/169171-MS>
- Mosavat N, Abedini A, Torabi F (2014) Phase behaviour of CO<sub>2</sub>-Brine and CO<sub>2</sub>-Oil Systems for CO<sub>2</sub> storage and enhanced oil recovery: experimental studies. Energy Procedia 63:5631–5645. <https://doi.org/10.1016/j.egypro.2014.11.596>
- Mutailipu M, Liu Y, Jiang L, Zhang Y (2019) Measurement and estimation of CO<sub>2</sub>-brine interfacial tension and rock wettability under CO<sub>2</sub> sub- and super-critical conditions. J Colloid Interface Sci 534:605–617. <https://doi.org/10.1016/j.jcis.2018.09.031>
- Nojabaei B, Johns RT, Chu L (2013) Effect of capillary pressure on phase behavior in tight rocks and shales. SPE Reserv Eval Eng 16:281–289. <https://doi.org/10.2118/159258-PA>
- Pan B, Li Y, Wang H, Jones F, Iglauer S (2018) CO<sub>2</sub> and CH<sub>4</sub> wettabilities of organic-rich shale. Energy Fuels 32:1914–1922. <https://doi.org/10.1021/acs.energyfuels.7b01147>
- Perera M, Gamage R, Rathnaweera T, Ranathunga A, Koay A, Choi X (2016) A review of CO<sub>2</sub>-enhanced oil recovery with a simulated sensitivity analysis. Energies 9:481. <https://doi.org/10.3390/en9070481>
- Prusty BK (2008) Sorption of methane and CO<sub>2</sub> for enhanced coalbed methane recovery and carbon dioxide sequestration. J Nat Gas Chem 17:29–38. [https://doi.org/10.1016/S1003-9953\(08\)60022-5](https://doi.org/10.1016/S1003-9953(08)60022-5)
- Rani S, Padmanabhan E, Prusty BK (2019) Review of gas adsorption in shales for enhanced methane recovery and CO<sub>2</sub> storage. J Pet Sci Eng 175:634–643. <https://doi.org/10.1016/j.petrol.2018.12.081>
- Rezk MG, Foroozesh J (2019) Phase behavior and fluid interactions of a CO<sub>2</sub>-Light oil system at high pressures and temperatures. Heliyon 5:e02057. <https://doi.org/10.1016/j.heliyon.2019.e02057>
- Saad SMI, Neumann AW (2016) Axisymmetric drop shape analysis (ADSA): an outline. Adv Colloid Interface Sci 238:62–87. <https://doi.org/10.1016/j.cis.2016.11.001>
- Samara H, Jaeger P (2021) Driving mechanisms in CO<sub>2</sub>-assisted oil recovery from organic-rich shales. Energy Fuels 35:10710–10720. <https://doi.org/10.1021/acs.energyfuels.1c01525>
- Samara H, Ke L, Ostrowski TV, Ganzer L, Jaeger P (2019) Unconventional oil recovery from Al Sultani tight rock formations using



- supercritical CO<sub>2</sub>. *J. Supercrit. Fluids* 152:104562. <https://doi.org/10.1016/j.supflu.2019.104562>
- Saraji S, Piri M, Goual L (2014) The effects of SO<sub>2</sub> contamination, brine salinity, pressure, and temperature on dynamic contact angles and interfacial tension of supercritical CO<sub>2</sub>/brine/quartz systems. *Int J Greenh Gas Control* 28:147–155. <https://doi.org/10.1016/j.ijggc.2014.06.024>
- Schön JH (2011) Pore space properties, in: *Handbook of petroleum exploration and production*. Elsevier, pp. 17–73. [https://doi.org/10.1016/S1567-8032\(11\)08002-5](https://doi.org/10.1016/S1567-8032(11)08002-5)
- Sharifigaliuk H, Mahmood SM, Al-Bazzaz W, Khosravi V (2021) Complexities driving wettability evaluation of shales toward unconventional approaches: a comprehensive review. *Energy Fuels* 35:1011–1023. <https://doi.org/10.1021/acs.energyfuels.0c03661>
- Sheng JJ (2015) Enhanced oil recovery in shale reservoirs by gas injection. *J Nat Gas Sci Eng* 22:252–259. <https://doi.org/10.1016/j.jngse.2014.12.002>
- Sheng JJ (2020) Introduction to shale and tight reservoirs, In: *Enhanced Oil Recovery in Shale and Tight Reservoirs*. Elsevier, pp. 1–6. <https://doi.org/10.1016/B978-0-12-815905-7.00001-3>
- Shojai Kaveh N, Barnhoorn A, Wolf K-H (2016) Wettability evaluation of silty shale caprocks for CO<sub>2</sub> storage. *Int J Greenh Gas Control* 49:425–435. <https://doi.org/10.1016/j.ijggc.2016.04.003>
- Song B, Springer J (1996) Determination of interfacial tension from the profile of a pendant drop using computer-aided image processing. *J Colloid Interface Sci* 184:77–91. [https://doi.org/10.1016/S0021-9797\(96\)90598-6](https://doi.org/10.1016/S0021-9797(96)90598-6)
- Stark PH, Chew K, Fryklund B (2007) The role of unconventional hydrocarbon resources in shaping the energy future, In: *International petroleum technology conference*. Presented at the international petroleum technology conference, Dubai, U.A.E. <https://doi.org/10.2523/IPTC-11806-MS>
- Surampalli RY, Zhang TC, Tyagi RD, Naidu R, Gurjar BR, Ojha CSP, Yan S, Brar SK, Ramakrishnan A, Kao CM (2015) Carbon capture and storage: physical, chemical, and biological methods. *American Society of Civil Engineers (ASCE)*
- Tao Z, Clarens A (2013) Estimating the carbon sequestration capacity of shale formations using methane production rates. *Environ Sci Technol* 47:11318–11325. <https://doi.org/10.1021/es401221j>
- Teklu TW, Alharthy N, Kazemi H, Yin X, Graves RM, AlSumaiti AM (2014) Phase behavior and minimum miscibility pressure in nanopores. *SPE Reserv Eval Eng* 17:396–403. <https://doi.org/10.2118/168865-PA>
- Tovar FD, Eide O, Graue A, Schechter DS (2014) Experimental investigation of enhanced recovery in unconventional liquid reservoirs using CO<sub>2</sub>: a look ahead to the future of unconventional EOR, in: *SPE unconventional resources conference*. Presented at the SPE unconventional resources conference, Society of Petroleum Engineers, The Woodlands, Texas, USA. <https://doi.org/10.2118/169022-MS>
- Wang J, Ryan D, Szabries M, Jaeger P (2019) A study for using CO<sub>2</sub> to enhance natural gas recovery from tight reservoirs. *Energy Fuels*. <https://doi.org/10.1021/acs.energyfuels.8b04464>
- Wang X, Luo P, Er V, Huang S-SS (2010) Assessment of CO<sub>2</sub> Flooding Potential for Bakken Formation, Saskatchewan, In: *Canadian unconventional resources and international petroleum conference*. Presented at the Canadian unconventional resources and international petroleum conference, society of petroleum engineers, Calgary, Alberta, Canada. <https://doi.org/10.2118/137728-MS>
- Yang D, Gu Y (2005) Interfacial interactions between crude oil and CO<sub>2</sub> under reservoir conditions. *Pet Sci Technol* 23:1099–1112. <https://doi.org/10.1081/LFT-200035536>
- Yang D, Tontiwachwuthikul P, Gu Y (2005) Interfacial interactions between reservoir brine and CO<sub>2</sub> at high pressures and elevated temperatures. *Energy Fuels* 19:216–223. <https://doi.org/10.1021/ef049792z>
- Yang Z, Liu X, Hua Z, Ling Y, Li M, Lin M, Dong Z (2015) Interfacial tension of CO<sub>2</sub> and crude oils under high pressure and temperature. *Colloids Surf Physicochem Eng Asp* 482:611–616. <https://doi.org/10.1016/j.colsurfa.2015.05.058>
- Yassin MR, Begum M, Dehghanpour H (2017) Organic shale wettability and its relationship to other petrophysical properties: a Duvernay case study. *Int J Coal Geol* 169:74–91. <https://doi.org/10.1016/j.coal.2016.11.015>
- Yekeen N, Padmanabhan E, Sevo TA, Kanesen KA, Okunade OA (2020) Wettability of rock/CO<sub>2</sub>/brine systems: a critical review of influencing parameters and recent advances. *J Ind Eng Chem* 88:1–28. <https://doi.org/10.1016/j.jiec.2020.03.021>
- Yekeen N, Padmanabhan E, Abdulelah H, Irfan SA, Okunade OA, Khan JA, Negash BM (2021) CO<sub>2</sub>/brine interfacial tension and rock wettability at reservoir conditions: a critical review of previous studies and case study of black shale from Malaysian formation. *J Pet Sci Eng* 196:107673. <https://doi.org/10.1016/j.petrol.2020.107673>

**Publisher's Note** Springer Nature remains neutral with regard to jurisdictional claims in published maps and institutional affiliations.